The impact of Borexino on the solar and neutrino physics

Gianpaolo Bellini

Istituto Nazionale di Fisica Nucleare, via Celoria 16, 20133 Milano, Italy

Abstract

The Borexino detector is characterized by a very low background level due to an unprecedented radio-purity, which allows to study the entire spectrum of solar neutrinos from very low energies ($\sim$150 keV). The solar neutrino rates from pp, ^{7}Be, pep, ^{8}B (with a threshold down to 3 MeV) and a stringent limit of the CNO cycle rate have been already measured. In addition evidences of a null day/night asymmetry and of the solar neutrino flux seasonal variation have been reached.

The contribution provided until now by Borexino in understanding the neutrino oscillation phenomenon concerns the first evidence of the oscillation in vacuum and the determination of the ν_e survival probability in vacuum: these results validate the paradigmatic MSW model in the vacuum regime.

The Borexino results are also in good agreement with the Standard Solar Model predictions, but the metallicity puzzle is still unsolved. In addition the pp flux measured by Borexino shows a good agreement with the Solar luminosity.

Evidence of geo-neutrinos has been also obtained at the level of 5.9σ C.L.

Borexino is still taking data in order to: upgrade the precision of the solar neutrino rates already measured, increase the sensitivity to the neutrino flux from the CNO cycle and hopefully measure it (very challenging), and test the existence of very short base-line neutrino oscillations.

E-mail address: gianpaolo.bellini@mi.infn.it.

1. Introduction

Borexino, installed at the Gran Sasso laboratory (Hall C), is continuously taking data since May 2007, with the exception of the period: May 2010–October 2011, when a further radio-purification of the scintillator has been carried out to suppress or reduce the residual contaminants, which survived the initial purification (during the detector filling). The data collected from May 2007 to May 2010 (the so called phase 1) have been already analyzed, reaching several results which are breakthroughs in the neutrino and in the Sun physics. The data taken until now during the phase 2 (which started in October 2011), and partially analyzed, have been provided already important results, but other challenging efforts are in progress.

The key constraints for the Borexino detector were dictated by the experiment goal to study the solar neutrinos with a threshold at 150–200 keV, a study never carried out before in real time by other experiments. In order to achieve this goal, the required radio-purity level of the detecting material (liquid scintillator) has to be 9–10 orders of magnitude lower than the natural ambient radioactivity. With the techniques developed during a long and intense period of R&D effort, Borexino reached and exceeded this goal, achieving unprecedented levels of radio-purity which allowed for the first time to measure in real time the neutrino rates produced by the pp, ^{7}Be, pep solar reactions and to reach a stringent upper limit for the CNO cycle.

2. The detector

Borexino is a scintillator detector, which employs a mixture of Pseudocumene (PC; 1,2,4 trimethylbenzene) and a fluorescent dye PPO (2,5 diphenyloxazole) at a concentration of 1.5 g/l. Borexino is designed following the basic requirement to keep the radioactivity at a very low level, and is based on the principle of graded shielding; it consists of concentric shells of increasing radio-purity, with the highest one at the center where the liquid scintillator core is placed. In Fig. 1 the detector design and layout are shown. Starting from outside, a water tank (WT) contains a stainless steel sphere (SSS) surrounded by 2100 m^3 of highly purified water. The SSS supports 2212 Photomultipliers (PMTs), coupled to optical concentrations (30% of optical coverage), and contains a nylon vessel (IV), 300 m^3 of volume, surrounded by 1050 m^3 of pseudocumene (buffer liquid), an aromatic chosen also as a diluent of the two component liquid scintillator inserted into the IV. The light emitted by the scintillator is detected by 2212 PMTs (Inner Detector – ID). The nylon wall of the IV is 125 μm thick and, as a consequence, the buoyancy on it has to be very small: so the density of the external shielding liquid is only slightly different from the one of the internal scintillator. A second nylon balloon functions as a barrier against the ^{222}Rn emitted mostly by the PMTs. In the buffer of Pseudocumene, 5 g/l of a quencher (DMP) is added to withdraw the scintillating power of the Pseudocumene alone.

Finally between the SSS and the WT, 208 PMTs assure the cosmic muon identification by exploiting the Cherenkov light produced in the highly purified water of the Water Tank (Outer Detector – OD).

The choice of the liquid scintillation technique was dictated by the high light-yield of the scintillator (50 times more than in the Cherenkov technique), and thus a good energy resolution. However, to the contrary of water Cherenkov detectors, the information on the incident neutrino direction is lost.

For more details see Refs. [1,2].

To cope with the goal of a very low radioactive background, many tools have been used during the installation. The crude oil for the Pseudocumene preparation has been procured from old
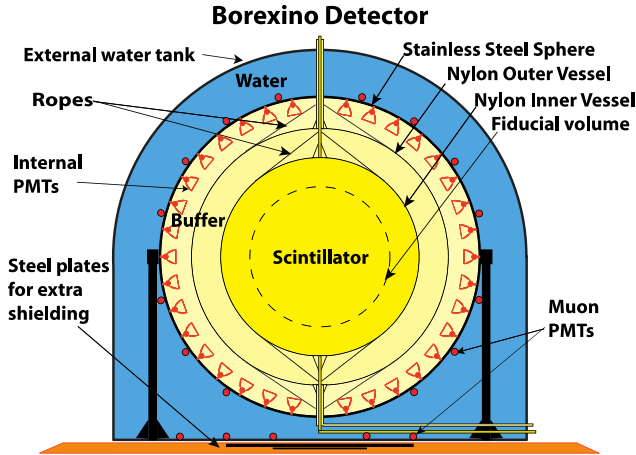
Borexino Detector

Fig. 1. Schematic layout of the Borexino detector.

layers to keep as low as possible the presence of ^{14}C, which is produced by the cosmic rays. All detector materials have been selected measuring their radioactivity. All stainless steel surfaces, lines, walls, fittings, valves have been electro-polished and the vessel nylon has been selected and extruded in clean room. Any operation has been carried out in clean rooms or in N_2/Ar atmosphere and the SSS itself has been equipped as a clean room of class 10 000. The PMTs have been developed in collaboration with a British firm using very low radioactive glass and ceramics. The Pseudocumene has been purified via water extraction, distillation at relatively low temperature, stripping with N_2, ultrafiltration. The Nitrogen for the stripping has been treated in cryogenic way to reduce the presence of ^{222}Rn, ^{39}Ar, ^{85}Kr [3] to unprecedented levels.

The radio-purity of Borexino, as measured at the beginning of the data taking, is summarized in Table 1, where it is compared with the regular radio-purity of the materials. It is possible to notice that in general the levels achieved are even better than the design goal [4].

The neutrino signals observed in the Borexino detector are due to the electrons recoiled in the elastic scatterings $\nu - e^-$ (the "neutrino energy spectrum" means in this text the energy spectrum of the electron recoil from the $\nu - e^-$ elastic scattering). The antineutrino interactions are well tagged trough the inverse β decay reaction $\bar{\nu} + p \rightarrow e^+ + n$ by two 0.511 MeV γs (prompt signal) plus a 2.2 MeV γ (delayed signal): the positron annihilates with the emission of two 0.511 keV γs, while the neutron is captured, with a delay due to the neutron thermalization time in the scintillator, of ∼250 µs, by a proton producing a deuteron and with the emission of the 2.2 MeV γ.

An extended calibration has been carried out in Borexino during 2009 and 2010 by means of: 11 artificial γ sources, a ^{222}Rn source consisting of a scintillator ^{222}Rn loaded vial, a ^{241}Am–^{9}Be neutron source covering an energy range from 122 to 4946 keV. The sources have been placed in the center of the IV and in various off-center positions, via a movable arm, to tune the light yield, the absolute energy scale, the spatial uniformity of the energy response, the position reconstruction, the α/β discrimination, and to check and tune the Monte Carlo simulations.

Following this calibration campaign the position reconstruction is now $\sigma(x, y, z) = 10$–12 cm; the light yield, 511 photoelectrons/MeV $\pm 1.5\%$; the energy resolution, $5\%/(E[\text{MeV}])^{1/2}$ in the range 200–2000 keV (beyond 2 MeV the resolution is a little worse because of the smaller variety of calibrating source energies).

Table 1

The radiopurity in the Borexino scintillator, gases and water used for the radio-purification (g/g = grams of contaminants over grams of material; cpd = counts per day).

Radio-isotope		Concentration or flux		Final
Name	Source	Typical	Required	Achieved
^{14}C	Intrinsic scintillator	$\sim 10^{-12}$ ^{14}C/^{12}C	$\sim 10^{-18}$ ^{14}C/^{12}C	$\sim 2 \times 10^{-18}$ ^{14}C/^{12}C
^{238}U	Dust, particulate,	10^{-5}–10^{-6} g/g	$<10^{-16}$ g/g	$(5.0 \pm 0.9)10^{-18}$ g/g
^{232}Th	All materials			$(3.0 \pm 1.0)10^{-18}$ g/g
^{7}Be	Cosmogenic	$\sim 3 \times 10^{-2}$ Bq/t	$<10^{-6}$ Bq/t	not observed
^{40}K	Dust, PPO	$\sim 2 \times 10^{-6}$ g/g (dust)	$<10^{-18}$ g/g	not observed
^{210}Po	Surface contamination	Decaying with a half time of ~ 138 days	<700 cpd/100 t	May 2007:500 cpd/100 t
				May 2009: 15 cpd/100 t
^{222}Rn	Emanation from materials, rock	10 Bq/l air, water	<10 cpd/100 t	<1 cpd/100 t
		100–1000 Bq/kg rock		
^{39}Ar	Air, cosmogenic	17 mBq/m^3 (air)	<1 cpd/100 t	$\ll 1$ cpd/100 t
^{85}Kr	Air, nuclear weapons	~ 1 Bq/m^3 (air)	< 1 cpd/100 t	30 ± 5 cpd/100 t

Table 2

Improvements of the scintillator radio-purity after the purification campaign during May 2010–October 2011.

Nuclide	Rate (cpd/100 t)
^{85}Kr	1 ± 9 cpd/100 t
^{232}Th equiv.	$<7.2 \times 10^{-19}$ g/g
^{238}U equiv.	$<9.5 \times 10^{-20}$ g/g
^{210}Bi	20 ± 2.2 cpd/100 t

The further purification carried out in continuous mode in the time period May 2010–October 2011 reduces ^{85}Kr, ^{210}Bi, ^{232}Th and U equivalents, as shown in Table 2.

3. The background

3.1. The residual contaminants

Despite the unprecedented radio-purity of Borexino, some contaminants are still remaining in the detector (Internal Background – IB), as:

- **^{85}Kr**, a β emitter with an end point at ~ 750 keV, present in Borexino during the phase 1 and at a level almost negligible in the phase 2, after the further purification of the scintillator; it is present in the air at the level of 1 Bq/m^3. This background falls on the ^{7}Be neutrino energy window.
- **^{210}Po**, an α emitter at 5.3 MeV, quenched in the scintillator of a factor ~ 10, and **^{210}Bi**, a β emitter with $Q = 1.16$ MeV. They are produced continuously by a residue of ^{210}Pb, but this is only one of the components producing the ^{210}Po rate; a second component is inserted every time operations on the scintillator are carried out. The ^{210}Po is probably embedded

in the inner walls of the pipes and is extracted by the scintillator that flows in them. As a consequence the ^{210}Po is not in equilibrium with ^{210}Bi and its second component (due to the operations on the scintillator) decays with 138.376 days half time. The ^{210}Po decay product has an energy falling just on the ^{7}Be neutrino energy region (taking into account the quenching factor), while the β from ^{210}Bi has a spectrum partly overlapped with the CNO and pep neutrino energy spectra.

- ^{14}C, a β emitter with a nominal end point at 156 keV; it is present in the crude oil and cannot be rejected via purification, but its contamination in the scintillator is at relatively very low level, even if it is the major contributor to the Borexino total counting rate. Its spectrum interferes with the pp neutrino energy spectrum.

Cosmogenic unstable nuclides are produced by the muons survived after the Gran Sasso overburden crossing; in the Hall C their rate is 1.1 muons/m^2 h. The most important of the cosmogenic nuclides is:

- ^{11}C, produced by the muon interactions on the ^{12}C of the scintillator at a rate of $28.5 \pm 0.2 \pm 0.7$ cpd/100 t. Due to its short half time (20.334 min) an equilibrium is settled between production and decay, producing a background more or less constant. ^{11}C decays into ^{11}B + e$^+$ + ν; ^{11}B has a very long lifetime ($\sim 10^9$ yr), while the positron annihilates producing a prompt signal in the energy region of CNO and pep neutrinos.

External γ-rays, survived though the detector shielding, contribute to the background in the scintillator (External Background – EB); they are emitted mainly by the vessel support structure, the PMTs, the light concentrators and the IV nylon walls (the most important are due to ^{208}Tl and ^{214}Bi decays). Their impact is very weak at low energy, while in the higher energy region the EB interferes with the ^{8}B neutrino study.

In order to have a better control of the external background a fiducial volume (FV) has been software defined within the IV as a 3 m radius sphere; later, due to some IV deformation, the FV became a volume with virtual walls away 1.5 m from the IV walls. A further cut is introduced in the vertical axis to shield the radiation emitted by the Inner Vessel reinforcements. Then the FV contains $\sim$75.5 t in $\sim$86 m^3 of volume.

The purification campaign via stripping and water extraction, carried out in the period May 2010–October 2011, reduced the residual contaminants (see Table 2); how they interfere with the neutrino solar signals is shown in Figs. 3, 4, 5.

3.2. Software tools to reject the residual background

The study of the residual background is successful in the Borexino detector, mainly due to its spectroscopic capability.

α/β discrimination. The scintillator used in the Borexino detector shows different decay times when excited by α particles or by β/γ. In order to discriminate between α and β/γ signals the G parameter [5] is used, which evaluates the different probabilities of the two signal types. This parameter is very efficient at an energy >500 keV, while at lower energy the separation between α and β/γ is not so sharp. Another method useful to reject the α signals is the subtraction from the event sample of a number of events equivalent to the area below the G distribution for αs.

Delayed coincidences. The natural radioactivity is dominated by the ^{232}Th and ^{235}U families (also ^{40}K contributes to the natural radioactivity, but its signal is negligible in Borexino). Seven and eight nuclides in the ^{232}Th and ^{235}U chains, respectively, decay emitting an α, which can be identified via the α/β discrimination; α emitters which can be preceded by a β/γ emitter (with continuous spectra). Just an example: the ^{214}Bi decays into β/γ with a maximum energy of $\sim$3.2 MeV, followed, after 164 µs, by the ^{214}Po decay into a 7.8 MeV α (quenched in the scintillator with a factor $\sim$10). Therefore these contaminants can be easily identified via a delayed coincidence between the correlated α and β/γ decays.

Statistical subtraction. Assuming the secular equilibrium, at least in the same family segment, it is possible evaluate the decay rates of nuclides connected with the ones involved in the delayed coincidences, and subtract their signals. It is the case for instance of the ^{232}Th and ^{235}U families, which are monitored via the ^{212}Bi–^{212}Po and the ^{214}Bi–^{214}Po delayed coincidences, respectively: measuring these delayed coincidences it is possible to evaluate the rate of ^{214}Pb and ^{212}Pb.

^{85}Kr. It can be identified with a direct fit on the energy spectrum and via its well tagged decay into excited ^{85}Rb, with the emission of a 173 keV β, followed, after 1.464 µs (lifetime), by the ^{85}Rb decay to the ground state, with a 514 keV γ emission; the branching ratio of this decay channel is 0.46%. Using the statistics of the entire phase 1, the Kr decay rate can be quoted as $30 \pm 5.3 \pm 1.5$ cpd/100 t, in agreement with the independent evaluation obtained through a fit on the event energy spectrum (Fig. 4). In the Borexino phase 2 the ^{85}Kr contamination is basically negligible.

^{11}C. The ^{11}C nuclides are identified and rejected via two selections. The first is a three-fold coincidence (TFC) involving the incident muon, the annihilation of the positron emitted in the ^{11}C decay (prompt signal) and, after $\sim$250 µs (delayed signal), a 2.2 MeV γ ray, which follows the capture of a thermalized neutron(s) produced in the 95% of the primary muon interactions. This coincidence involves software space and time cuts, as a cylindrical veto of 80 cm around the muon track and a further spherical veto of 1 m radius around the positron annihilation point, which coincides with the muon interaction point. This veto, prolonged during $\sim$2 h after the muon interaction (and then the neutron production), is very efficient, but reduces the fiducial exposure. A further event discrimination is obtained using a pulse shape analysis via a boosted-decision-tree algorithm (BTD), which exploits the different profiles of the reconstructed emission times of the positron and of the electron: the β^+ annihilation in two back-to-back γ rays needs, on the average, longer time, due to the formation, in 50% of the cases, of the ortho-positronium; in addition the β^+ topology is multi-side distributed due to the 2γs showers.

In Fig. 5 the fit results are shown before and after that the TFC selection would be applied.

Other cosmogenic unstable nuclides. Other nuclides are produced by cosmic muons. Many of them have a Q-value higher than the solar neutrino energy spectrum and/or show a very low rate. Only ^{10}C, ^{7}Be and ^{6}He have to be considered: for the first a procedure similar to the ^{11}C case can be used; regarding the others, their rates are calculated via Monte Carlo simulations and then subtracted.

^{14}C. Its β-spectrum ends at 156 keV and, even taking into account the smearing due to the resolution, it has a very small impact on the ^{7}Be neutrino measurement, while it is the main background in the study of the neutrino rate from pp (see Fig. 3).

^{210}Po. The α/β discrimination is very effective in reducing this background.

^{210}Bi. The ^{210}Bi is always present in the scintillator and its rate is measured directly. In phase 2 its rate is $\sim$20 cpd/100 t; it does not show specific tags and its energy spectrum falls just in the CNO (and pep) energy region. While the spectrum of the electrons recoiled from the pep $\nu_e - e^-$
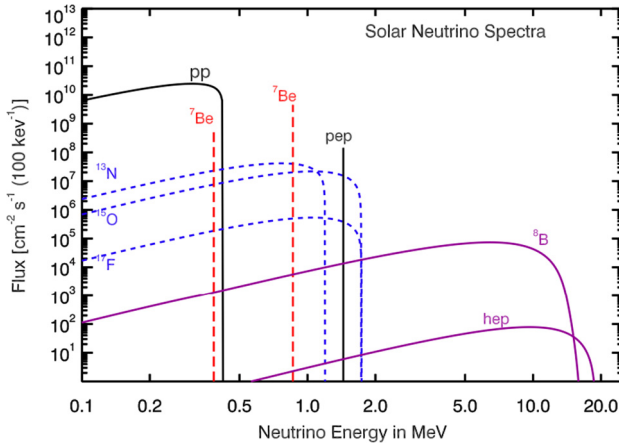
Fig. 2. The Solar neutrino spectrum as foreseen from the Standard Solar Model (Bahcall and Pinsonneault).

interactions is well tagged due to the Compton edge (pep neutrinos are mono-energetic), the CNO energy distribution shows a shape very similar to the ^{210}Bi spectrum. Therefore the only way to measure the CNO neutrino rate is to know exactly the ^{210}Bi rate studying the ^{210}Po decay (see § 3.1). The ^{210}Po rate versus time has to show two components: an exponential $(\exp(t/\tau_{Po}))$ for the ^{210}Po introduced during the scintillation movements, plus a flat contribution due to the continuous ^{210}Po (and ^{210}Bi) production from the ^{210}Pb decay. Therefore, in principle, it is possible to measure the ^{210}Bi rate via the ^{210}Po decay and then subtract it from the CNO-like events (see § 9) [6].

4. The experimental measurements in the solar sector

The goal of Borexino is to measure separately the absolute rates of the solar neutrinos as produced by the various nuclear reactions taking place in the Sun. In Fig. 2 the solar neutrino fluxes, as foreseen by the Solar Neutrino Model (SSM), are shown; the pp chain produces ∼99% of the entire solar energy and the remaining ∼1% is produced by the CNO cycle [7].

The SSM, developed during decades by J. Bahcall and M. Pinsonneault and coworkers uses as input data the solar luminosity, the mass and radius of the Sun, the ratio Z/X (the so called *metallicity*) between C, N, O, Ne, Mg, Si, Ar, Fe and the hydrogen present on the surface. The conservation laws and the energy transport equations are applied. The SSM predictions can be checked via the helioseismology (sound-waves speed profiles) and the neutrino fluxes measured experimentally. In the last decade a metallicity puzzle has arisen: the chemical composition of the photosphere is obtained from its spectral lines: a data treatment in 1D [8] shows a very good agreement with the helioseismology; on the other hand a more refined treatment in 3D, done later [9], gives a lower metallicity with respect to the previous one ($Z/X = 0.0178$ with respect to 0.0229), but with the new metallicity value the SSM is unable to reproduce properly the helioseismology observations. The neutrino fluxes change depending on the adopted metallicity value [10,11].

The Cerenkov experiments measured the tail of the neutrino spectrum from ^{8}B reaction, which represents ∼0.01% of the total solar neutrino rate. The main problem which forbids to these experiments to measure the low energy part of the spectrum is the natural radioactivity of the
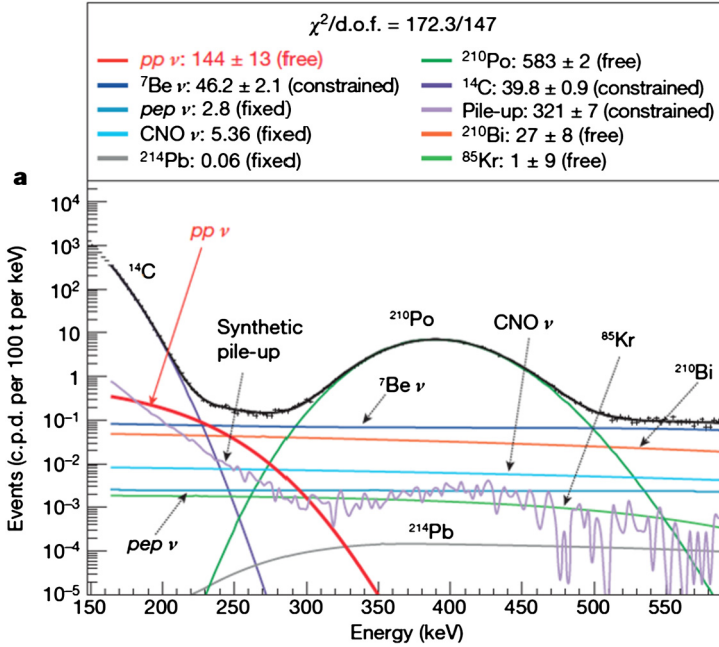
Fig. 3. Borexino fit on the solar neutrino energy spectrum between 165 and 590 keV. All rates are in cpd/100 t. The pp-neutrino component is in red. The values of the rates of the other components are quoted above the plot (see also the text).

detector components. In the following the Borexino results of the various solar flux study are shown.

pp. Borexino performed the first real time measurement of the pp neutrinos [12] analyzing the data collected during 408 days of the phase 2 (January 2012–May 2013). According to the Physics World (IOP) this result has been nominated among the Top 10 Breakthroughs of 2014. The main problem in measuring the solar neutrinos from pp is the β spectrum produced by the ^{14}C decay (despite its low contamination, $\sim 2 \times 10^{-18}$ ^{14}C/^{12}C in the scintillator) with an end point at 156 keV Q-value, partially overlapped with the pp spectrum, which has an end point at 264 keV. A correlated problem is done by the pile-up uncorrelated events either between two ^{14}C events or between one ^{14}C event and one pp neutrino event, which are measured as a single event occurring in a very short time window; the pile-up component can be determined independently, using a data-driven method, which has been called "synthetic pile-up" [12]. In Fig. 3 the final fit on the energy spectrum in the range 165–590 keV shows the interference among pp, ^{14}C and the other residual contaminants (see the insert above the figure), the ^{214}Po α energy spectrum included (the α/β discrimination is not applied in this fit).

We have to note also that the contributions of pp, ^{210}Po, ^{210}Bi, ^{85}Kr (consistent with zero) are left free in the fit, while ^{7}Be, ^{14}C and the pile-up are constrained at values measured independently; the ^{214}Pb rate is fixed at the values determined by means of the ^{214}Bi(β)–^{214}Po(α) correlated coincidences. Finally pep and CNO neutrino contributions are fixed following the SSM expectations, taking into account the values of the neutrino oscillation parameters [10]: this choice is justified by the very little contribution of pep and CNO in the energy region of interest. In addition many fits have been performed varying the fixed parameters: the very little changes
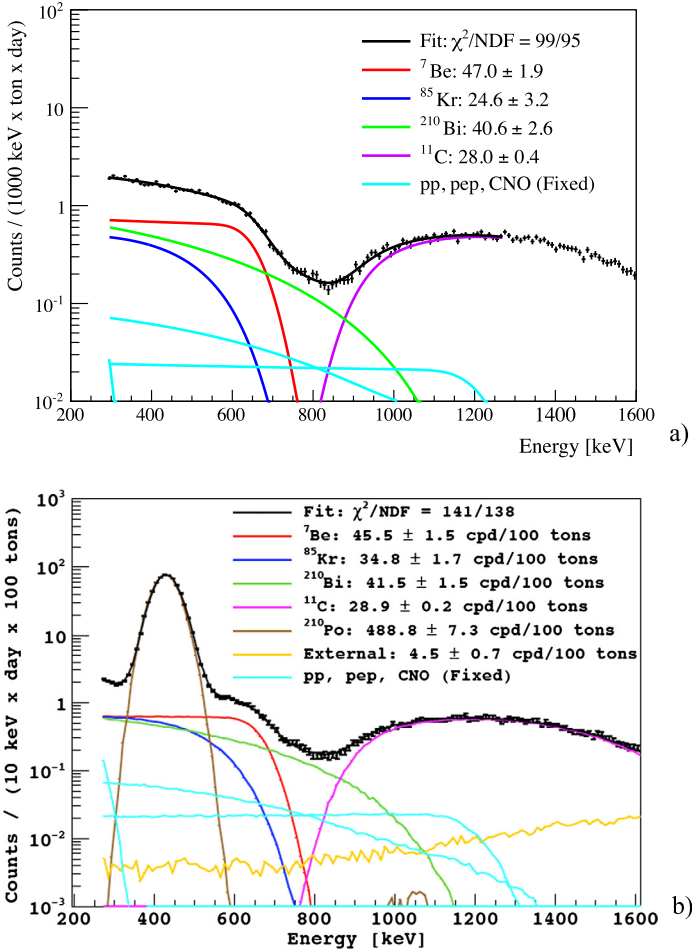
Fig. 4. (a) Fit over 200–1270 keV energy range, after the α subtraction (see text), to extract the ^{7}Be solar neutrino interaction rate. The fit is done via an analytical approach. (b) Monte Carlo based fit over 270–1600 keV; a soft α cut is applied via the G parameter.

($<$1%) resulted from these fits have been quoted in the pp systematic errors. The measured neutrino rate from pp is 144 ± 13 (stat.) ± 10 (sys.) cpd/100 t and the related electron–neutrino survival probability is 0.64 ± 0.12. Taking into account the neutrino oscillation parameters the measured solar pp neutrino flux is $(6.6 \pm 0.7) \times 10^{10}$ cm^{-2} s^{-1} (the statistical and systematic errors are added in quadrature).

^{7}Be. The rate of the solar neutrinos from ^{7}Be reaction at 862 keV has been measured two times, already after 192 [13] and then after 740.6 [14] live days of data taking during the phase 1. The results of the fit on the energy spectrum of the recoiled electrons are shown in Figs. 4a and 4b. The fits are carried out with both an analytical approach (Fig. 4a) and by means of Monte Carlo simulations (Fig. 4b). In the fit ^{7}Be, ^{85}Kr, ^{210}Bi, ^{11}C, ^{210}Po are left free while pep and CNO are fixed according to the SSM-high metallicity [10] (the pep and CNO show a very little rate with respect to ^{7}Be). In the plot of Fig. 4a the α contribution is subtracted evaluating the

area below the α G distribution, while in Fig. 4b the αs are subtracted with a soft application of the G parameter. In both the plots the ^{7}Be energy spectrum (in red) is easily identified due to the Compton-like shoulder at ∼660 keV. The two approaches used in the fits give the same result: 46 ± 1.5 (stat.) ± 1.5 (syst.) cpd/100 t and the equivalent flux, considering the 3-flavor neutrino oscillations, is $(4.43 \pm 0.22) \times 10^9$ cm^{-2} s^{-1}.

The day/night asymmetry has been also measured in the ^{7}Be energy region. It is defined as: $A_{ND} = 2\frac{R_N - R_D}{R_N + R_D}$, where R_N and R_D are respectively the night and day ^{7}Be-neutrino counting rates. The data have been collected during 757.8 live days. They have been corrected to take into account the seasonal variation of the Earth–Sun distance, which can mimic the day/night effect because its impact on the day and night rates is not uniform [15]. The result rules out any day/night difference: $A_{ND} = 0.001 \pm 0.012$ (stat.) ± 0.007 (syst.).

pep and **CNO.** The energy region over ∼0.8 MeV up to ∼2 MeV is dominated by ^{11}C cosmogenic background; over 1700 keV some contribution of the external background is also present. The ^{11}C background is partly rejected via the TFC (see § 3): it is reduced to ∼5% with an exposure reduced to 48.5%. The fitting strategy makes use of a binned maximum likelihood multidimensional fit on the events surviving the TFC selection and, at the same time, on the rejected events, constraining the non-cosmogenic species to be the same, because uncorrelated with the vetoes. The fit is performed simultaneously on the energy spectrum, on the radial distribution and on the pulse shape BDT parameter (see § 3), with different fitting ranges (see Fig. 5 (top)): the BDT reduces further the ^{11}C survived after the TFC rejection. The second important background is due to ^{210}Bi, which falls just in the pep and CNO energy region, and shows a shape similar to the CNO one. Just because of the shape similarity between CNO and ^{210}Bi, the fit on the CNO flux is very difficult; the estimation of its upper limit has been carried out fixing the pep rate at the SSM prediction. The measured pep rate is 3.1 ± 0.6 (stat) ± 0.3 (syst) cpd/100 t and the corresponding flux is $(1.63 \pm 0.35) \times 10^8$ cm^{-2} s^{-1} [16].

In Fig. 5 (bottom) the pep energy spectrum is shown, once subtracted the considered background: the fit is compared with it. The Compton-like edge of the electrons recoiled from the elastic scattering with the mono-energetic pep neutrinos is well visible; the hypothesis of absence of pep neutrino signal, analyzed via a likelihood test, is rejected at 97% C.L.

The CNO rate upper limit has been obtained via a fit, where pep rate has been fixed at its value, leading to a CNO rate <7.4 cpd/100 t and a CNO solar flux <7.7 × 10^8 cm^{-2} s^{-1}.

^{8}B. The ^{8}B neutrino rate has been measured by Borexino with a threshold down to 3. MeV of the recoiled electrons, which corresponds to ∼3.2 MeV of the neutrino energy [17]. The fits have been performed on the radial distribution and not on the energy spectrum as in the case of the mono-energetic neutrinos, because the shape of the ^{8}B continuous spectrum is influenced by the neutrino oscillation. The data over 3 MeV are almost unaffected by the contaminants present in the scintillator with the exception of ^{208}Tl, which is a member of the ^{232}Th family with a Q value of ∼2.8 MeV. It is subtracted statistically via the identification of the ^{210}Bi–^{210}Po correlated signals. Further background is due to neutrons produced by muon interactions and muon induced radioactive nuclides: both are rejected by a proper time veto after each crossing muons. The measured ^{8}B rate is 0.22 ± 0.04 (stat.) ± 0.01 (syst.) cpd/100 t; the flux is $(2.4 \pm 0.4 \pm 0.1) \times 10^6$ cm^{-2} s^{-1} in agreement with the data from SNO and Superkamiokande.

Seasonal modulation. The solar neutrinos flux shows an annual variation induced by the change of the distance Earth–Sun due to the eccentricity of the Earth orbit. This variation is expected to follow a sinusoidal shape with one year period and a maximum flux difference of ∼7%. This effect has been studied with Borexino, using the ^{7}Be neutrino interaction rate, on the data collected during three years of the phase 1 [19]. Unfortunately the statistics of three years
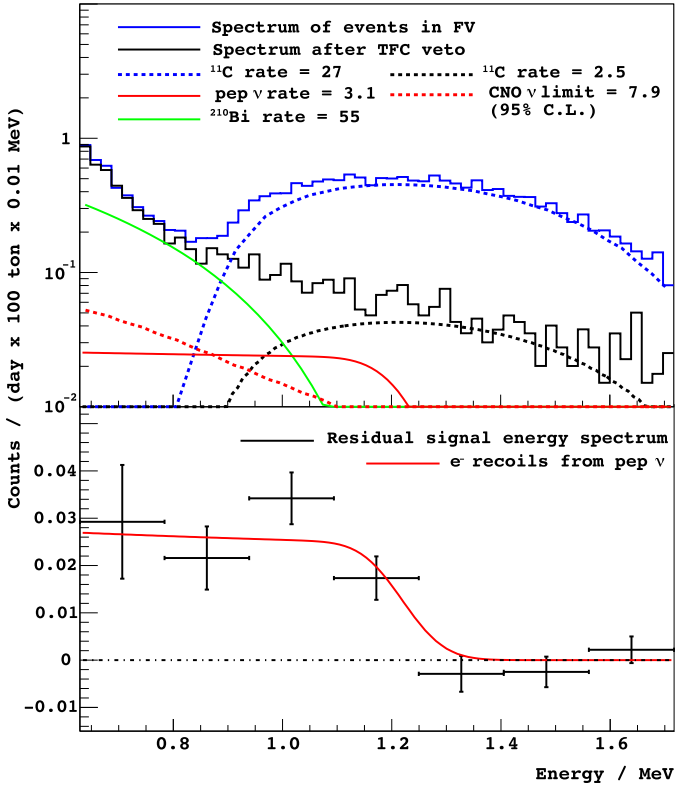
Fig. 5. Energy spectrum to study the pep and CNO solar neutrino fluxes. Top: Energy spectra before (blue solid line) and after (black solid line) the application of the TFC veto. The dashed blue and black lines show the ^{11}C rates before and after the TFC veto. The ^{210}Bi is shown by the green line, while the solid red and the dashed red are the best fit on the pep neutrino spectrum and the upper limit of the CNO neutrinos, respectively. The rates, integrated over the entire spectrum, are quoted in cpd/100 t. Bottom: Energy spectrum of the data (black crosses), once subtracted the contribution of all fitted background components, compared to the pep spectrum (red line). The expected Compton edge is evident.

is not enough to allow independent spectral fits in year portions chosen in order to have in the same time a meaningful statistics, and the reproduction of the sinusoidal annual modulation. The analysis of the phase 2 data, now in progress, is very promising, but it is not yet completed and the results not yet released.

Three different approaches have been used; two of them are reported here: fit versus time and Lomb–Scargle method [18]. With respect to the selection of the events for ^{7}Be rate measuring there are two changes: the fiducial volume has been enlarged to 145 t (which includes events that are far away from the vessel walls of more than 0.5 m), and a "strong" application of the α subtraction has been adopted even if it involves a not negligible reduction of the β events. This last cut eliminates also the background due to ^{210}Po, which is not stable due to scintillator movements [19].

The instabilities of ^{210}Bi and ^{222}Rn have significant impact on this analysis. The fluctuations of the ^{210}Bi rate are software compensated, while the presence of ^{222}Rn, introduced during hardware operations, forced to discard some period of data taking. Therefore this analysis refers to the statistics collected in the period January 2008–May 2010.
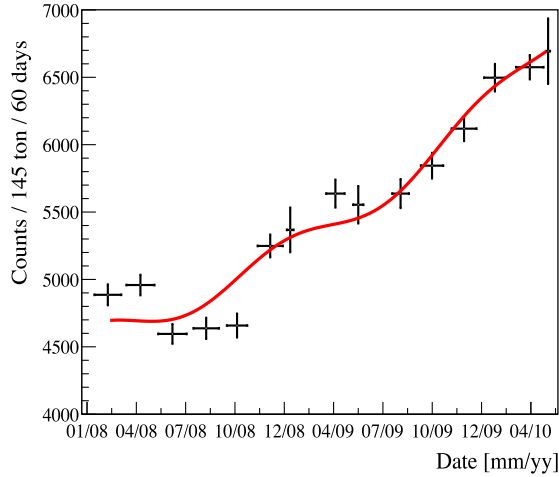
Fig. 6. Result of the analysis of the seasonal variation following the approach "rate versus time". The expected curve is compared to the experimental data 60-days binned. (For interpretation of the references to color in this figure legend, the reader is referred to the web version of this article.)
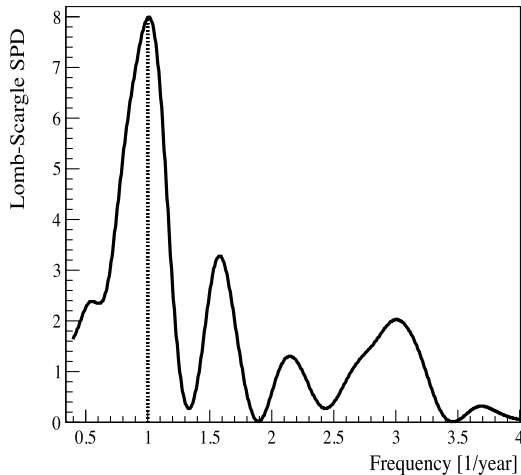

Fig. 7. The Lomb–Scargle periodogram. The Spectral Power Density is quoted on the vertical axis.

For the fit on the rate versus time the data are grouped in bins 60-days long. The result is shown in Fig. 6. The period and the phase are close to the expected value of 1 ± 0.07 yr.

The Lomb Scargle approach [18], an extension of the Fast Fourier Transform, allows to analyze data samples with time gaps and is able to give the statistical significance of the analyzed periods. For this analysis the events are grouped in bins of 10 days. In Fig. 7 the Lomb–Scargle periodogram shows a clear peak corresponding to 1 yr. At a frequency of 1 yr, the Spectra Power Density (SPD), which is the value of the periodogram, is 7.961.

In Fig. 8 the hatched area shows the SPD obtained with 10^4 simulations assuming no seasonal variation of the solar neutrino signal, while the plot extended up to 8 SPD represents the results of similar simulations, but adopting the hypothesis of the seasonal variation. From the plot we
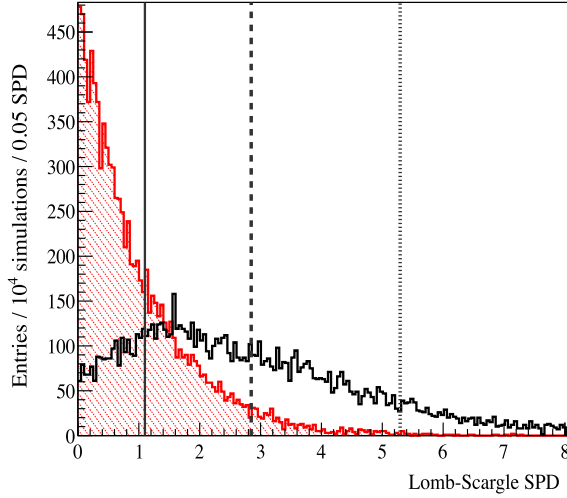
Fig. 8. The plot extended up to 8 SPD is the distribution of the Lomb–Scargle Spectral Power Density for frequency of 1 yr, as obtained with 10^4 Monte Carlo simulations of the seasonal variation, background included. The hatched area represents the same simulations but without any seasonal variation. The vertical axes are the sensitivity threshold of 1σ (continuous line), 2σ (dashed line), 3σ (dotted line). The detected SPD of 7.961 corresponds to an evidence with a significance higher than 3σ. (For interpretation of the references to color in this figure legend, the reader is referred to the web version of this article.)

can observe that the SPD of 7.691, as achieved with the Borexino data, shows evidence of annual modulation with a significance higher than 3σ.

5. Impact on the neutrino physics

The Borexino results are important insights in the neutrino physics, in particular on the oscillation phenomenon, but not only.

The null result obtained in the analysis of the day/night asymmetry rejects (at 8.5σ) the LOW solution on the "Δm^2 versus $\tan^2\theta_{12}$" plane; this result is obtained by considering only the solar results, without using the reactor antineutrino data and therefore without assuming the CPT symmetry. In Fig. 9 (left panel) a global analysis is shown, which takes into account the radio-chemical, Superkamiokande Phase I and III [20] and the SNO-LETA data [21]. We can observe that in this case the LOW region is still present at 99.73% C.L.; to rule out it completely the Kamland reactor antineutrino data have to be included in the fit. In the right panel of Fig. 9 the Borexino data (and then the day/night result) are included in the solar global fit and the LOW region is ruled out at 8.5σ C.L.

The ν_e survival probability versus the neutrino energy is a useful way to compare the experimental data with the model expectations. This comparison with the paradigmatic MSW-LMA model before Borexino is shown in Fig. 10. The model was validated at high neutrino energy, corresponding to the oscillation matter enhanced, by SNO and Superkamiokande, but at low energy and on the transition region the comparison is very weak. Borexino succeeded to observe for the first time the oscillation in vacuum measuring the pp neutrino survival probability (0.64 ± 0.12) and to determine the ratio between the survival probabilities in vacuum (0.29 ± 0.10) and in matter, using pp and ^{8}B, this last measured by Borexino above 3 MeV. This ratio turns out to be $= 2.2 \pm 0.86$.
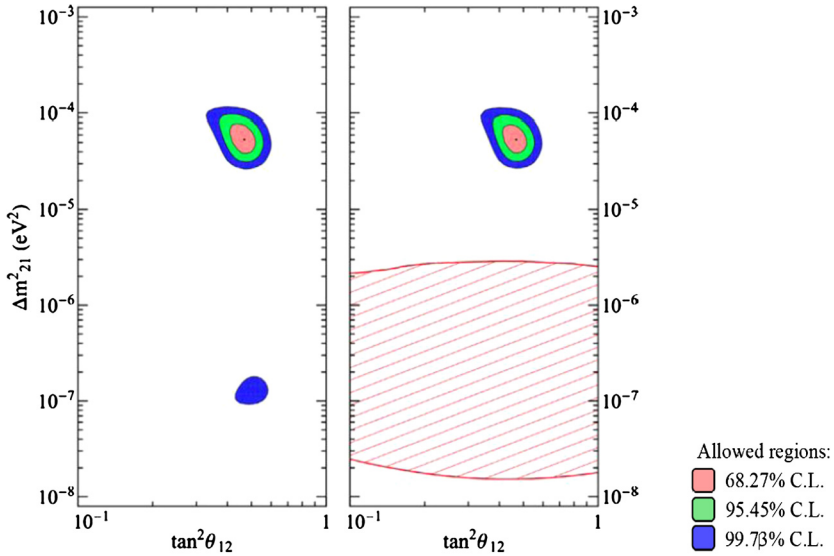
Fig. 9. Neutrino Oscillation parameter estimation with a global fit. At left the global fit takes into account all solar data with the exclusion of Borexino: the LOW region is still present. At right the same fit includes also Borexino data: the hatched area is excluded at 99.73%, ruling out the LOW region at 8.5σ C.L. (For interpretation of the references to color in this figure legend, the reader is referred to the web version of this article.)
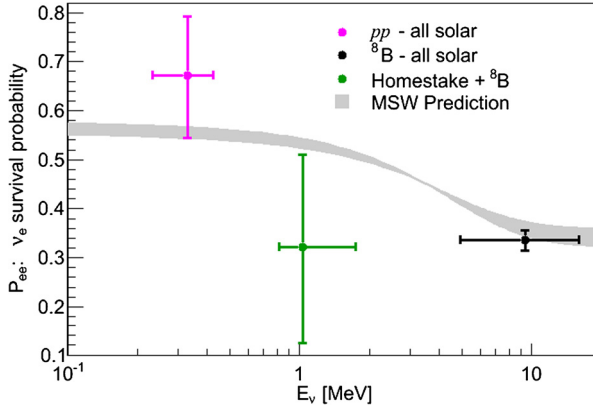

Fig. 10. ν_e survival probability before Borexino. The band is 1σ prediction from the MSW-LMA model; the right point, the SNO-Superkamiokande result; the other two points are obtained by Gallex/GNO, SAGE and Homestake data, once subtracted the ^{8}B flux. The left point is the pp flux evaluation while the point in the middle is an average among ^{7}Be, pep, CNO fluxes. (For interpretation of the references to color in this figure legend, the reader is referred to the web version of this article.)

In Fig. 11 the survival probability versus energy of the ν_e produced by the nuclear reactions in the Sun includes the Borexino results as obtained up to now. The experimental data are compared with the MSW-LMA predictions.

An important point concerning the transition region is the presence of the so called "up-turn" in passing from the matter regime to the transition region towards the low energies. SNO
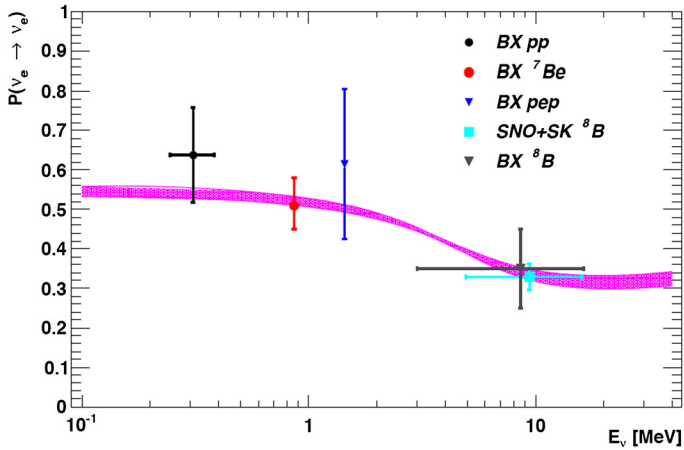
Fig. 11. ν_e survival probability including the results reached by Borexino until now. The violet band is the MSW-LMA prediction (1σ); all data points are measured by Borexino except the light blue, which refers to the SNO+Superkamiokande ^{8}B results. The vertical error bars correspond to 1σ; the horizontal uncertainty is the neutrino energy range used in the analysis.

Leta, Superkamiokande and Borexino have not enough statistics to reach some conclusion, but presently the up-turn is slightly disfavored (at the level of 1–1.7σ).[1]

The transition region study is important for the search of new physics. Its shape is influenced by the Non-Standard neutrino Interaction (NSI) hypothesis [22], but the differences in the transition region shape with and without the NSI hypothesis are not so relevant and then very high precision measurements are needed to distinguish between them and the MSW-LMA expectations. The study of a possible NSI can be done more easily analyzing the energy spectrum of the recoiled electron from the $\nu - e$ scattering [23], in particular for the ^{7}Be neutrinos, which is monoenergetic and does not need of convolution with the incident neutrino spectrum, as for instance is the case of ^{8}B. Some bounds have been already imposed by various experiments on solar, atmospheric and reactor (anti)neutrinos [24]. In Borexino, the limitation to this analysis comes from the residual background, especially ^{85}Kr, and, to lesser extend, from ^{210}Bi, which can mimic non-zero values of the NSI parameters ε_{eR} and ε_{eL} [23]. Until now an analysis has been completed only for the data of Borexino phase 1 and it gives results already significant in imposing bounds on the NSI parameters (see Fig. 12). In § 8 a prediction of what can be achieved with the data of phase 2 is shown.

The transition region and the "up turn" can be strongly influenced also by the existence of an ultra-light sterile neutrino [25].

6. Impact on the Solar physics

Solar neutrinos are the proof that nuclear fusion reactions are the source of the Solar energy. Borexino has provided for the first time the direct experimental evidence that the prediction of the SSM for the pp-ν flux, which produces ~99% of the solar power, is correct, as far as the SSM expectations for the two components of the pp chain: ^{7}Be and pep.

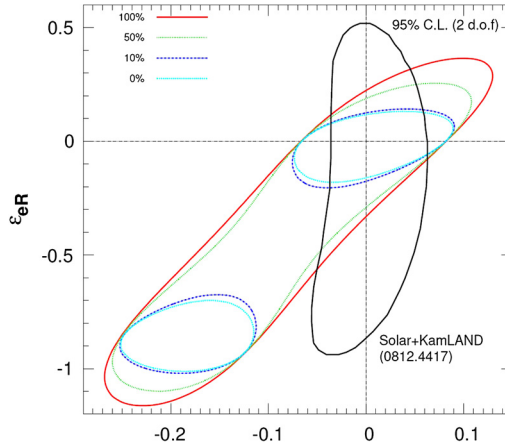[1] See talks at TAUP 2015 of Livia Ludhova and Hiroyuki Sekiya.

Fig. 12. Scatter plot of the NSI parameters: ε_{eR} vs ε_{eL} [23]. The bound from the global fit solar + Kamland is in black; the solid red curves indicate the bounds obtained with the Borexino phase 1 data, while the other colored curves show how the allowed regions can be further limited if in the Borexino data the ^{85}Kr is 100%, 50%, 10%, 0%, of the background present in the phase 1. The region allowed is the common area of the black and the red curves.

Table 3
Comparison of the solar neutrino fluxes measured by Borexino with the SSM expectations and a global fit which includes all experimental results obtained with solar, reactor, accelerator neutrinos.

Solar neutrino flux	GS98 (cm^{-2} s^{-1}) high metallicity $Z/X = 0.0229$	AGS09 (cm^{-2} s^{-1}) high metallicity $Z/X = 0.0178$	Experimental results (Borexino)	Global fit including solar, reactor, accel. data [11] (cm^{-2} s^{-1})
pp	$5.97\,(1 \pm 0.007) \times 10^{10}$	$6.04\,(1 \pm 0.007) \times 10^{10}$	$6.6\,(1 \pm 0.106) \times 10^{10}$	$5.97^{+0.037}_{-0.033} \times 10^{10}$
^{7}Be	$5.00\,(1 \pm 0.07) \times 10^{9}$	$4.56\,(1 \pm 0.07) \times 10^{9}$	$4.43 \pm 0.22 \times 10^{9}$	$4.80^{+0.24}_{-0.22} \times 10^{9}$
pep	$1.44\,(1 \pm 0.012) \times 10^{8}$	$1.47\,(1 \pm 0.012) \times 10^{8}$	$1.63 \pm 0.35 \times 10^{8}$	$1.448 \pm 0.013 \times 10^{8}$
^{13}N	$2.96\,(1 \pm 0.14) \times 10^{8}$	$2.17\,(1 \pm 0.14) \times 10^{8}$		$\leq 13.7 \times 10^{8}$
^{15}O	$2.23\,(1 \pm 0.15) \times 10^{8}$	$1.56\,(1 \pm 0.15) \times 10^{8}$	$<7.7 \times 10^{8}$ total CNO	$\leq 2.8 \times 10^{8}$
^{17}F	$5.52\,(1 \pm 0.17) \times 10^{8}$	$3.40\,(1 \pm 0.16) \times 10^{8}$		$\leq 8.5 \times 10^{7}$
^{8}B	$5.58\,(1 \pm 0.14) \times 10^{6}$	$4.59\,(1 \pm 0.14) \times 10^{6}$	$5.2 \pm 0.3 \times 10^{6}$	$5.16^{+0.13}_{-0.09}\,^{+0.30}_{-0.26} \times 10^{6}$

As it is well known the neutrinos promptly escapes from the Sun's core, while the photons need $\sim 100\,000$ yr to escape. Therefore the comparison between neutrino and photon luminosity tests the solar stability at 10^5 yr time scale and gives the direct proof that the pp chain provides almost the total solar energy. The comparison is carried out by comparing the rates of the solar nuclear reactions as calculated from the luminosity[2] and from the neutrino fluxes: a good agreement between the two rates has been found.

The fluxes of the solar neutrinos measured by Borexino are summarized in Table 3, where they are compared with the SSM predictions with high and low metallicity, and with the results of a global fit [11] which includes the data of the radiochemical experiments, the various phases of the Cherenkov experiments, Borexino and Kamland, the experiments considered in NuFit [26],

---

[2] The total power of the Sun is 3.84×10^{33} erg per second.

Minos, T2K, Chooz, Palo Verde, Double Chooz, Daya Bay, Reno. From these data it is possible to conclude that the Borexino results confirm the SSM predictions and are in good agreement with the results of the global fit. On the other hand the results obtained up to now are not enough to fix the metallicity puzzle due to the incertitude of the model and the experimental errors. We have to note that the Borexino results are not constrained by the solar luminosity, at the contrary of the global fit.

7. Geoneutrinos

Geo-neutrinos, electron anti-neutrinos, are produced in the β-decays of ^{40}K and of several nuclides in the chains of the long-lived radioactive isotopes ^{238}U and ^{232}Th, which are naturally present in the Earth. The Earth emits geo-neutrinos with a flux of about $10^6\,cm^{-2}\,s^{-1}$. Radioactive nuclides decay into α particles, electrons, antineutrinos and emit energy: 51.7 MeV from the ^{238}U and 42.8 MeV from the ^{232}Th chains; ^{40}K produces 1.32 MeV. Therefore the released radiogenic heat and the geo-neutrino flux are in a well fixed and known ratio. If we assume the chondritic ratio, it is possible in principle to determine the amount of radiogenic heat contributing to the total terrestrial surface heat flux (Urey ratio) by measuring the geo-neutrino flux. This is the main goal of the geo-neutrino study, which provides also important inputs for many geophysical and geochemical models of the Earth. Therefore geo-neutrinos can be used as a unique direct probe of the Earth interior, not accessible by any other means.

In the liquid scintillator (of Borexino and Kamland) a geo-neutrino (anti-neutrino) interacts with a proton via the inverse beta decay reaction (see § 2) with a threshold at 1.8 MeV; therefore Borexino in unable, as the detectors liquid scintillator based, to detect the antineutrino emitted by ^{40}K.

The geo-neutrinos have been highlighted by Kamland in 2005 (C.L. $< 2\sigma$) and in 2008 with a C.L. of $\sim 2.5\sigma$, by Borexino in 2010 with a C.L. $> 4\sigma$ [27]. Later Kamland showed a signal with null hypothesis of the geo-neutrino existence having a probability of $\sim 2 \times 10^{-6}$ [28]. Finally Borexino in 2015 has published an evidence for geo-neutrinos at 5.9σ C.L. and a null hypothesis with a probability of 3.6×10^{-9} [29].

The main background for the geo-neutrinos is represented by the antineutrinos from nuclear reactors and the detector radioactivity. In both cases Borexino is favored due to the low reactor antineutrino flux at the Gran Sasso site and the unprecedented detector radiopurity. The reactor antineutrino flux has been evaluated using the IAEA and EdF data bases and taking into account all important parameters concerning 194 European plus 246 extra-Europe reactors. In Fig. 13 the best evidence of geo-neutrinos reached up to now is shown [29].

The data are fitted using an unbinned maximum likelihood with geo-neutrinos and reactor antineutrinos as free parameters, while the radioactive background (actually mostly negligible) is constrained. Two types of fit have been carried out: 1) Th/U mass ratio is fixed to the chondritic value of 3.9; 2) U and Th are taken as free parameters. The number of events quoted in Fig. 13 has been obtained via the fit 1). The best fit event number from the reactor antineutrinos is in agreement with the evaluations obtained using the IAEA and EDF data bases.

The Borexino results bring the following hints:

1) The evaluation of the geo-neutrino signal from the mantle is obtained by subtracting the crust contribution from the measured signal. At the Gran Sasso site the crust signal has
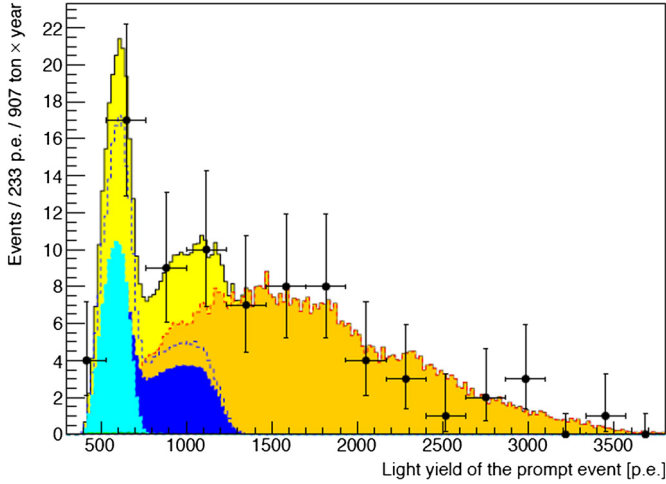
Fig. 13. Fit on the selected antineutrino spectrum: black points = data - - - - - = best fit U + Th with fixed mass chondritic ratio (Th/U = 3.9): $N_{geo}^{events} = 23.7^{+6.5}_{-5.7}$ (stat.)$^{+0.9}_{-0.6}$ (syst.), $S_{geo} = 43.5^{+11.8}_{-10.4}$ (stat)$^{+2.7}_{-2.4}$ (syst)TNU, $N_{reactor}^{events} = 52.7^{+8.5}_{-7.7}$ (stat)$^{+0.7}_{-0.9}$ (syst), blue area = U free parameter light blue area = Th free parameter - - - - - = Reactor neutrinos.

been evaluated to be $S_{crust} = 23.4 \pm 2.8$ TNU[3] and then $S_{mantle} = 20.9^{+15.1}_{-10.3}$ TNU. The null hypothesis of the presence of radioactive nuclides in the mantle is rejected at 98% C.L.

2) The radiogenic heat represents an important part of the total Earth's energy budget. From the Borexino data the radiogenic heat ranges between 23 and 36 TW and, considering 1σ interval, between 11 and 52 TW. The large range is due to the various assumptions on the radioactive nuclide distribution in the mantle: either homogeneously diffused or accumulated close the border mantle-core. If the chondritic mass ratio and the ratio $m(K)/m(U) = 10^4$ are assumed, the radiogenic heat is $= 33^{+28}_{-20}$ TW. The radiogenic contribution has to be compared with the evaluated total Earth's heat, which ranges from 31 to 47 TW.

3) For the first time it is possible to observe two well separated picks in the geo-neutrinos energy range, produced by ^{232}Th and ^{238}U. The peak distribution at lower energy is due to both ^{232}Th and ^{238}U (see black dashed line in Fig. 13); the bump at higher energy is due only to ^{238}U and the light blue is due only to ^{232}Th.

The uncertainties of the experimental measurements of Borexino are dominated by the statistics; therefore to go from hints to evidences more statistics is needed.

8. What next

Borexino will take data until 2020 or so.

Its main goals are: to measure the solar neutrino flux produced by the CNO cycle, to increase the precision of the fluxes already measured in the phase 1, as ^{7}Be, pep, ^{8}B, to test the existence of the very short baseline neutrino oscillation and of the sterile neutrino via an artificial source (SOX).

---

[3] TNU = Terrestrial Neutrino Unit = 1 event/year/10^{32} proton, 100% efficiency.

In the theory of energy generation in stars two processes produce energy during the star main sequence lifetime: the proton–proton (p–p) chain which is the dominant energy source in stars like the Sun and lower mass stars, and the CNO cycle, which is considered to be the primary channel producing energy in stars more massive than 1.5 times the solar mass, but this hypothesis never has been tested and needs an experimental evidence. The only chance to confirm the existence of the CNO cycle is to study the solar flux, where the CNO cycle contributes only at the level of ∼1% of the total solar energy. Borexino started the study of the CNO cycle making an effort to measure with very high precision the ^{210}Bi rate. As explained in § 3.1 and 3.2 the exact knowledge of the ^{210}Bi rate is the only way to measure the CNO rate, and the present Borexino strategy is to determine it via the monitoring of the ^{210}Po rate versus time, which has to show an exponential ($\exp(t/\tau_{Po})$) plus a flat contribution due to the continuous ^{210}Po (and ^{210}Bi) production from the ^{210}Pb decay (see § 3.2) [8]. Until the beginning 2015, due to hardware operations and temperature changes in the Gran Sasso Hall C, where Borexino is installed, the ^{210}Po rate was high and variable, and therefore the data did not have enough sensitivity to allow the determination of any deviation from an exponential decay of the ^{210}Po rate versus time. But the situation is now different because the detector has been not and will not be disturbed during a long time, and in addition a thermal insulation around the Water Tank has been installed to avoid even very small (±0.1°) temperature changes. The temperature monitoring during the last months shows that the temperature is stabilized assuring an unavoidable requirement for the CNO flux measurement, which in any case is very challenging. Borexino plans in principle to take data for CNO until the end 2018.

Another Borexino effort is the analysis of the phase 2 data, collected during about four years. The goal is to measure with improved precision the solar fluxes already measured in the phase 1.

^{7}Be flux is planned to be measured with a total error of 3–4%. This achievement is important not only because we can do better that the present global analysis (see Table 2), but also because the exclusion plot for the neutrino NSI can be largely upgraded. In Fig. 14, the same plot of Fig. 12 is reproduced, assuming the background levels of the phase 2 (0% for ^{85}Kr and 20 ± 1.5 cpd/100 t for ^{210}Bi) and 3.6% of uncertainty for the ^{7}Be flux. The green curves are the regions allowed by the Borexino data, as expected from phase 2, and the red curves correspond to the assumption of a null rate for ^{210}Bi. Combining the results obtained by the other solar neutrino experiments plus Kamland (black line in Fig. 14), the only allowed region would be the area included in the upper green line, around $\varepsilon_{eR} = 0$ and $\varepsilon_{eL} = 0$.

The solution of the transition region upturn problem in the plot "ν_e survival probability versus neutrino energy" (see § 5) could be helped by the study of ^{8}B with higher statistics: the goal is to be able to quote the ^{8}B flux in the energy region 3–5 MeV with limited errors. The total uncertainty of the measured flux using the data of phase 1 is fully dominated by the statistical errors, while the systematic one is very limited. On the basis of pure statistical considerations, we expect to have, for the phase 2, a total error of ∼10% for the flux measured in the 3–5 energy range.

Borexino, is an ideal detector for a sterile neutrino experimental investigation testing the very short baseline neutrino oscillation using artificial sources. Therefore it has been decided to perform a campaign of measurements with one artificial external neutrino source (SOX) allocated in a tunnel present under the Borexino detector, which ends just below the detector center at 8.25 m from it. The source will be a ^{144}Ce–^{144}Pr activated at ∼5 Bq; it emits antineutrinos with a continuous energy distribution up to 3 MeV [30].

Borexino can study the short distance neutrino oscillations in two ways. The first is the standard *disappearance* technique used by many experiments at reactors, accelerators and with solar
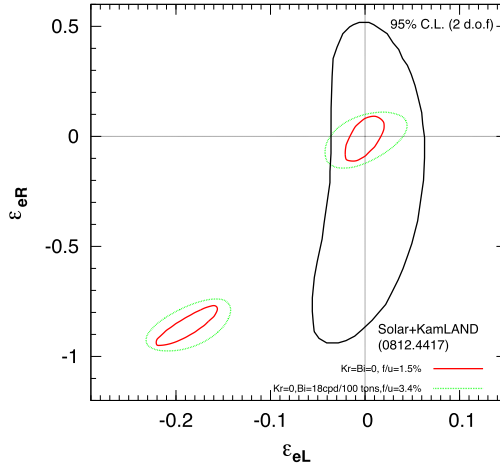
Fig. 14. Exclusion plot for the neutrino NSI. The green lines correspond to what can be expected by Borexino phase 2; for the red lines the ^{210}Bi contamination is assumed null. The black lines are the bounds imposed by the other solar experiments + Kamland. The allowed region corresponds to the green line, slightly reduced by the black one.

neutrinos: if oscillation occurs, the total count rate measured at a given distance from the source is lower than the one expected without oscillation. The second method concerns the possibility to observe directly the *oscillation waves* in the hypothesis of very short baseline oscillations and of the existence of a sterile neutrino. The expected Δm^2 is of the order of 1 eV^2 and the energy of neutrinos from the artificial source is of the order of few MeV; then the typical oscillations length is of the order of a few *m* and the oscillations waves can be directly "seen" in a large detector like Borexino, whose active diameter exceeds 6 m.

The data taking is planned to be carried out during 2017 and 2018, a period planned to take data also for the solar neutrinos: the two measurements are not incompatible (the antineutrino–electron elastic scattering can be precisely calculated and then subtracted).

The idea of this measurement campaign has been triggered by the claimed reactor anomaly and the deficit of the Gallex and Sage calibration sources [31] and especially by the results of MiniBooNE [32], sensitive to VSBL $\nu_\mu \to \nu_e$ (and $\bar{\nu}_\mu \to \bar{\nu}_e$) transitions and the longstanding LSND anomaly [33] which could suggest a third oscillation range at ~ 1 eV^2. It has to be note that the E/L ratio in SOX is very close to the same ratio in the MiniBooNE and LSND experiments.

Acknowledgements

References

[1] G. Alimonti, et al., Borexino Collaboration, Astropart. Phys. 16 (2002) 205.

 [2] G. Alimonti, et al., Borexino Collaboration, Nucl. Instrum. Methods A 600 (2009) 568.
 [3] G. Alimonti, et al., Borexino Collaboration, Nucl. Instrum. Methods A 609 (2009) 5.
 [4] C. Arpesella, et al., Borexino Collaboration, Astropart. Phys. 18 (2002) 1.
 [5] E. Gatti, et al., A Linear Method of Discrimination Between Elementary Particles in Liquid Scintillator, IAEA, Wien, 1965.
 [6] F.L. Villante, et al., Phys. Lett. B 701 (2011) 336.
 [7] J.N. Bahcall, Phys. Rev. C 65 (2002) 025801.
 [8] N. Grevesse, A.J. Sauval, Space Sci. Rev. 85 (1998) 161.
 [9] M. Asplund, N. Grevesse, A.J. Sauval, P. Scott, Annu. Rev. Astron. Astrophys. 47 (2009) 481.
[10] A.M. Serenelli, W.C. Haxton, C. Pena-Garay, Astrophys. J. 7432 (2011) 4.
[11] J. Bergstroem, et al., arXiv:1601.00972v1 [hep-ph], 5 Jan 2016.
[12] G. Bellini, et al., Borexino Collaboration, Nature 512 (2014) 383.
[13] C. Arpesella, et al., Borexino Collaboration, Phys. Lett. B 658 (2008) 101.
[14] G. Bellini, et al., Borexino Collaboration, Phys. Rev. Lett. 107 (2011) 141362.
[15] G. Bellini, et al., Borexino Collaboration, Phys. Lett. B 707 (1) (2012) 22.
[16] G. Bellini, et al., Borexino Collaboration, Phys. Rev. Lett. 108 (2012) 051302.
[17] G. Bellini, et al., Borexino Collaboration, Phys. Rev. D 82 (2010) 033000.
[18] N.R. Lomb, Astrophys. Space Sci. 39 (1976) 447;
     J.D. Scargle, Astrophys. J. 263 (1982) 835.
[19] G. Bellini, et al., Borexino Collaboration, Phys. Rev. D 89 (2014) 112007.
[20] K. Abe, et al., Superkamiokande Collaboration, Phys. Rev. D 83 (2011) 052010.
[21] K. Aharmin, et al., SNO Collaboration, Phys. Rev. C 81 (2010) 055504.
[22] Y. Minakata, C. Pena-Garay, arXiv:1009.4869v2, 2012, Special issue Neutrino Physics, Volume 2012 (2012), Article ID 349686, Hindawi, 2012.
[23] S.K. Agarwalla, F. Lombardi, T. Takeuchi, J. High Energy Phys. 12 (2012) 079, arXiv:1207.3492.
[24] A. Bolanos, et al., Phys. Rev. D 79 (2009) 113012.
[25] P.C. de Holanda, A.Yu. Smirnov, Phys. Rev. D 69 (2004) 113002;
     P.C. de Holanda, A.Yu. Smirnov, Phys. Rev. D 83 (2011) 113011.
[26] NuFIT webpage, http://www.nu-fit.org.
[27] S. Abe, et al., Kamland Collaboration, Phys. Rev. Lett. 100 (2008) 221803;
     G. Bellini, et al., Borexino Collaboration, Phys. Lett. B 687 (2010) 299.
[28] A. Gando, et al., Kamland Collaboration, Phys. Rev. D 88 (2013) 033001.
[29] M. Agostini, et al., Borexino Collaboration, Phys. Rev. D 92 (2015) 031101.
[30] G. Bellini, et al., J. High Energy Phys. 8 (2013) 038.
[31] J.N. Abdurashitov, et al., Phys. Rev. C 73 (2006) 045805;
     C. Giunti, M. Laveder, Phys. Rev. C 83 (2011) 065504 and the references therewith.
[32] A.A. Aguilar-Arevalo, et al., MiniBooNE Collaboration, arXiv:1207.4809.
[33] A. Aguilar, et al., LSND Collaboration, Phys. Rev. D 64 (2001) 112007.